Active diffusion and advection in the *Drosophila* ooplasm result from the interplay of the actin and microtubule cytoskeletons

Maik Drechsler[1,*] , Fabio Giavazzi[2,*], Roberto Cerbino[2,#] and Isabel M. Palacios[1,#]

1 – Department of Zoology, University of Cambridge, CB2 3EJ, Cambridge, UK

2 – Department BIOMETRA, University of Milan, Milan, Italy

* - These authors contributed equally to this work

- Shared last authorship and corresponding authors, mip22@cam.ac.uk and roberto.cerbino@unimi.it

Key words: *self-organization; active processes; motion; body plan; oogenesis; cell asymmetries; cytoskeleton; microtubules; actin; motor proteins*

SUMMARY (MAX 150 WORDS, NO REFERENCES)

Transport in cells occurs via a delicate interplay of passive and active processes including diffusion, directed transport and advection. Despite progresses in super-resolution microscopy, discriminating and quantifying these processes is a challenge, requiring tracking of rapidly moving, sub-diffraction objects in a crowded, noisy environment. Here we use Differential Dynamic Microscopy with different contrast mechanisms to provide a thorough characterization of the dynamics in the *Drosophila* oocyte. We study the motion of vesicles and the elusive dynamics of a cytoplasmic F-actin mesh, a known regulator of cytoplasmic flows. We find that cytoplasmic motility constitutes a combination of directed motion and random diffusion. While advection is mainly attributed to microtubules, we find that active diffusion is driven by the actin cytoskeleton, although it is also enhanced by the flow. We also find that an important dynamic link exists between vesicles and cytoplasmic F-actin motion, as recently suggested in mouse oocytes.

INTRODUCTION

The spatial distribution and organization of cytoplasmic content, like proteins or protein complexes, nucleic acids, and whole organelles require the combined action of passive and active biophysical processes. In fact, thermal-based diffusion is not sufficiently fast and effective in redistributing large organelles, like vesicles, within the cell (1). This is due to their large size, which makes their diffusion coefficient small, as well as to the typically crowded and viscous environment that is found inside cells. Active transport mechanisms mitigate the ineffectiveness of thermal diffusion. Molecular motor proteins carry attached cargos (such as organelles and vesicles) along cytoskeletal filaments, which act as tracks for directed (a.k.a. persistent or ballistic or super-diffusive) transport across the cell (2). In addition, in larger cells, it is likely that the transport of such cargoes causes a large-scale net flow, known as cytoplasmic streaming (3, 4). As a result of the viscous drag, caused by a translocating motor, streaming leads to a circulation of the cytoplasm and its efficient remixing (5, 6). Finally, recent studies demonstrate that ATP-dependent processes are responsible for the presence of random forces within the cytoplasm, whose effect leads to the displacement of tracer particles in a diffusive-like fashion - named active diffusion - that is more efficient than thermal-based diffusion (7-11). Understanding the details of the subtle interplay between all these processes is a demanding task, due to the many time- and length-scales and the multiple molecular pathways involved.

In this work, we study the interaction between different mechanisms of motion in the *Drosophila* oocyte. *Drosophila* oogenesis is well studied from a genetic point of view and the large oocyte can be probed with a variety of chemical treatments and microscopy tools. In the oocyte, microtubules and kinesin-1 are essential for both the transport of cargos and cytoplasmic streaming (12, 13). At mid-oogenesis (stage 9, st9), the topology and speed of cytoplasmic flows directly correlates with the topology of the microtubule cytoskeleton and the speed of kinesin, respectively (14). In addition, a cytoplasmic network of actin filaments (F-actin) - known as the actin mesh - is present within the oocyte and acts as a negative regulator of the microtubule/kinesin-dependent flow (15). However, much remains to be uncovered about the interplay between the actin mesh and the microtubule cytoskeleton in regulating the motion of material within the ooplasm. The recent discovery of a link between cytoplasmic actin and vesicle dynamics in mouse oocytes already suggests a close relationship between vesicle transport, motor activity and the actin cytoskeleton (16). However, it remains unclear whether this observation represents a general feature, also present in other eukaryotic cells.

To gain insight on these issues we simultaneously probed the dynamics of both cytoplasmic F-actin and vesicles in wild type oocytes, as well as in oocytes with aberrant cytoskeletons, and different cytoplasmic streaming conditions. We combined direct space methods, such as particle imaging velocimetry (PIV) and particle tracking (PT), with Differential Dynamic Microscopy (DDM) (17, 18). DDM probes the sample dynamics not in the direct space, but in the Fourier domain, with the bonus of being able to analyze densely distributed objects, whose size is well below the resolution limit of the microscope, and in the presence of substantial amounts of noise.

Using chemical treatment and genetic manipulation we can show that the dynamics of vesicles result from two contributes: a persistent ballistic motion due to cytoplasmic flows and a diffusion process of active nature. Surprisingly, we found that a similar combination of ballistic and diffusive movements also captures the dynamics of F-actin, showing a strong correlation between the actin and the vesicles motions. This result provides an important link between the active diffusion of vesicles and the underlying fluctuating non-equilibrium actin mesh, of which we quantify the overall dynamics by focusing in particular on the diffusive-like component. We discuss our results considering a recently proposed model for the dynamics of a particle embedded in a living cell, where both thermal fluctuations and non-equilibrium activity coexist (19).

We also demonstrate that, in our system, active diffusion constitutes an ATP-dependent process, with at least two distinct ingredients. On one hand the actin mesh itself seems to be a major source of active diffusion. However, we also find that microtubule based cytoplasmic flows enhance active diffusion, and only depletion of both cytoskeletons results in the abrogation of active diffusive-like motion. Therefore, our data outlines a key role of the dynamic cytoplasmic F-actin and microtubule cytoskeletons in driving the active diffusion motion of vesicles.

Overall, our findings show that: 1) the major ATP-dependent entities responsible for advection and active diffusion are the microtubule and cytoplasmic F-actin networks, and 2) an important dynamic link exists between vesicles and cytoplasmic F-actin motion, as recently found in mammals (16). This work also sheds new light into the dynamic interplay between ATP-dependent forces and cytoplasmic mechanics to regulate intracellular motility.

RESULTS AND DISCUSSION

Ooplasmic dynamics consist of persistent and diffusive motion

The asymmetric localization of developmental determinants by microtubule motors (such as kinesin-1) in the *Drosophila* stage9 (st9) oocyte is a key event for the specification of the body axes of the embryo (20). In addition, the translocation of cargos by kinesin-1 induces bulk movements of the cytoplasm – called cytoplasmic streaming or flows. These flows can be measured by particle image velocimetry (PIV), using endogenous vesicles as tracer particles (14). However, while PIV gives an accurate description of flow velocities and topology, it is unsuitable to describe non-persistent motion. Therefore, we used Differential Dynamic Microscopy (DDM) to monitor and characterize cytoplasmic movements in more detail (Fig. 1)(18, 21). Analyzing Differential Interference Contrast (DIC) time-lapse movies of living oocytes by DDM (DIC-DDM) unveiled a more complex dynamic behavior, which is not fully captured by PIV. In fact, DIC-DDM analysis shows that ooplasmic vesicles move in a ballistic, persistent, as well as in a random, diffusive manner (Fig. 1A,B).

In DDM experiments the dynamic motion is encoded in the so called intermediate scattering function f(q,Δt), which describes the relaxation of density fluctuations with wave-vector q as a function of the delay time Δt (Fig. 1E)(18, 22)In our experiments, the intermediate scattering functions are found to be well described by a simple advection-diffusion model

$$f(q,\Delta t) = p\left(\Gamma_1(q)\Delta t\right)\cdot e^{-\Gamma_2(q)\Delta t} \qquad (1)$$

in which the vesicles are subjected to a directional, ballistic motion with rate $\Gamma_1(q)$ as well as to a random, diffusive motion with rate $\Gamma_2(q)$. In this framework, each vesicle bears the same diffusivity D_{ves} ("ves" stands for vesicles) and a constant velocity drawn from a prescribed probability distribution function (see also Materials and Methods). We thus expect that $\Gamma_1(q) = v_{ves}q$, where v_{ves} is the average vesicle speed and $\Gamma_2(q) = D_{ves}q^2$. Fitting of the experimental intermediate scattering functions (Fig. 1E) to Eq. (1), confirmed the validity of our model and allowed the simultaneous determination of Γ_1 and Γ_2 for each q (Fig. 1F), that exhibited the expected ballistic and diffusive scaling. By repeating this analysis on N=7 cells (with an average of 1500 vesicles per cell contributing to the DIC-DDM signal) we obtained v_{ves} = 36±14 nm/s and D_{ves} = (3±1) 10^{-3} μm^2/s, where in both cases the deviation from the average represents the standard deviation of the population.

The ratio $r=6D_{ves}/v_{ves}\simeq 500$ nm corresponds to a characteristic length scale that separates two distinct regimes: over distances larger than r, advection is the most efficient transport mechanism, while on smaller length scales diffusion prevails. Of note, in our case r is roughly of the order of the vesicle radius. Therefore, it is not surprising that PIV, which operates over a coarse-grained grid with a resolution much larger than the size of the tracers, fails in capturing the erratic, small scale, diffusive movement. On the other hand, PIV can efficiently measure the persistent, large-scale motion of the vesicles, which can be used to validate our DIC-DDM approach. To this aim, we analyzed the same DIC movies by PIV (Fig. 1C). The comparison between DIC-DDM and DIC-PIV shows that both methods reveal the same quantitative description of flows. With DIC-PIV we find a mean vesicle speed $\overline{u}$ = 20±6 nm/s that is in very good agreement with the 2D projection of the 3D velocity v_{ves} obtained with DIC-DDM ($u_{ves}= 0.56*v_{ves}=20\pm7$ nm/s, Fig. 1C, see Materials and Methods for details). Comparable information can also be extracted by PIV analysis of movies obtained in reflection microscopy with vesicles that reflect light at 561nm (14). We find that each vesicle in the DIC images reflects light at 561nm from its center (Fig. 1B). Therefore, it is not surprising that using either DIC or reflection microscopy provides the same information regarding the vesicle motion (Fig. S1). More importantly, the nearly identical velocity values obtained by PIV or DDM support the hypothesis that the persistent movement of most vesicles is induced by the microtubule-dependent flows (14). However, compared to reflection imaging, DIC has three advantages for general studies on motion of cytoplasmic components. Firstly, the focal plane with DIC is thicker. Secondly, there is no need to use a specific laser line with DIC, and thus the number of fluorophores that can be combined with DIC is higher. And thirdly, DIC can theoretically be applied to any cell type.

In conclusion, our methods are non-invasive, as no tracer particles need to be injected into the cells, and, furthermore, we do not need to apply any external force to characterize the motion of cytoplasmic components. In addition, DDM can quantitatively separate the persistent, ballistic motion from the random, diffusive-like movement experienced by the same set of vesicles. More importantly, our results open to the possibility of a more sophisticated and detailed description of general intracellular motions.

The motility of cytoplasmic actin filaments directly correlates with vesicle motion

The cytoplasm constitutes a densely packed environment, containing not only organelles, but also highly dynamic actin filaments. After successfully using DDM to quantify the motion of vesicles, we applied it to monitor the motility of the cytoplasmic F-actin network traversing the oocyte cytoplasm. This task is made difficult due the small size of the filaments, their fast

and random movement, their crowding, and finally a low signal-to-noise ratio. Compared to vesicles, actin filaments exhibit a very different morphology and biomechanical properties, and have been found to be the source of active diffusion processes in various cell types (8, 23-25).

To understand the overall cytoplasmic dynamics in oocytes, we imaged vesicles (DIC) and F-actin simultaneously (Fig. 2A and Fig. S2). In st9 oocytes, a three-dimensional F-actin network traverses the entire cytoplasm (Fig. 2A-C and Fig. S2C) (15). This actin mesh is formed by the cooperative activity of two nucleators, Spire and the formin Capuccino (15, 26, 27). Staining fixed oocytes using the F-actin binding drug phalloidin shows the presence of intertwined filaments, as well as actin rich dots or foci (Fig. 2B and Fig. S2C). However, labeling actin in living cells by fluorescent tags has proven to be challenging and the overall motility of this structure is completely unknown. Yeast formins reject tagged actin monomers (28) - a fact we could confirm in *Drosophila* oocytes. Fluorophore-tagged Act5C (one out of six actin proteins in flies, and the only one expressed ubiquitously) becomes incorporated into cortical actin structures, but fails to be built into cytoplasmic filaments (Fig. S2B). Furthermore, fluorophore-tagged Act5C has a dominant-negative effect, preventing the formation of the actin mesh and inducing fast cytoplasmic flows ((29) and data not shown). Thus, in order to study the dynamics of the actin mesh, we used the F-actin binding protein UTRN.GFP, ubiquitously expressed under the *sqh* promotor (Fig. 1C) (30). UTRN.GFP consists of the calponin homology domain of human Utrophin fused to GFP, strongly binding to actin filaments, but not actin monomers (31). Based on fixed samples, UTRN.GFP has no effect on the morphology of the actin network, or on the timing of its formation and disappearance (Fig. S2C). Thus UTRN.GFP constitutes a suitable probe to visualize cytoplasmic F-actin in living oocytes.

Visual inspection of the movies reveals that cytoplasmic actin filaments are highly motile and seem to be dragged through the ooplasm in a random, “flowing” manner (Movie S1). Those movies also suggest that this F-actin structure does not constitute an interconnected stable meshwork of filaments, but rather resembles a network of constantly assembling and disassembling filaments, that may intertwine when in close proximity (Movie S1). Attempts to quantify the motion of the actin network by particle tracking or PIV were unsuccessful, mainly because of the large level of noise and crowding of the structure. Therefore, we combined DDM with confocal imaging (Con-DDM) (32) to assess the motility of this crowded and noisy actin structure. Notably, the same advection-diffusion model used for interpreting the motion of the vesicles is also found to accurately describe the dynamics of cytoplasmic F-actin (Fig. 2D). Fitting of the q-dependent relaxation rates $\Gamma_1 = v_{act}\, q$ and $\Gamma_2 = D_{act}\, q^2$

provides an estimate for the characteristic large-scale velocity v_{act} and for the effective diffusivity D_{act} of the actin filaments (where "act" stands for actin, Fig. 2E). Such effective diffusion is in principle a combination of the actual diffusion of the center of mass of actin filaments and of any active processes that reshape the actin network.

The quantities v_{ves}, D_{ves}, v_{act}, D_{act}, display some variability from cell to cell, but exhibit interesting correlations. In fact, comparing the results of actin with those on vesicles revealed that the large-scale velocity v_{act} in each cell compares very well with the vesicle velocity v_{ves} (Fig. 2F), as $v_{act} \simeq v_{ves}$. This result indicates that both actin and vesicles move in a persistent manner by advection, most likely because of microtubule-dependent flows. In addition, we found a remarkable correlation between the diffusion coefficient of vesicles and the effective diffusivity of F-actin, as $D_{act} \simeq 2D_{ves}$ (Fig. 2G). This correlation, which will be discussed in more detail below, suggests the existence of an important dynamic link between vesicles and cytoplasmic F-actin motion. This hypothesis is compatible with recent findings in mouse oocytes, where it is found that the actin mesh is made of actin filaments that polymerize from the surface of vesicles (16, 33).

Persistent motion enhances active diffusion

As for the link between diffusion and flow, our results suggest that the diffusive motion of vesicles and actin filaments results from the combination of an intrinsic component and of a flow-dependent contribution, which is evident when plotting the diffusion coefficient D of either the vesicles or actin as a function of the corresponding velocity v (Fig. 2H). The linear dependence of D_{ves} on v_{ves} is well captured by the fitting function $D_{ves} = D_{ves,0}(1+a_{ves}v_{ves})$ with $D_{ves,0}=(1.2\pm0.5)\ 10^{-3}\ \mu m^2/s$ and $a_{ves}=(2\pm1)\ 10^{-2}\ s/\mu m$, where $D_{ves,0}$ is the diffusion coefficient for the intrinsic component and $1/a_{ves}=50\ \mu m/s$, the typical velocity above which flows considerably affect diffusion. Notably, the flow-independent diffusion coefficient $D_{ves,0}$ is significantly larger than the thermal diffusion coefficient $D_{TH}=3.1\ 10^{-4}\ \mu m^2/s$ (TH for thermal) that can be estimated for vesicles in the oocyte (average size $1\pm0.2\ \mu m$), based on previous measurement of the viscosity (η=1.4 Pa s) for these oocytes (horizontal dotted line in Fig. 2H) (14). We can thus conclude that $D_{ves,0}$ describes an active diffusion process, devoid of any flow contributions.

Similar results are also found for actin, since the effective diffusivity $D_{act}= D_{act,0}(1+a_{act}v_{act})$ is made of an intrinsic and a flow-dependent contribution, with $D_{act,0}=(3\pm1)\ 10^{-3}\ \mu m^2/s$ and $a_{act}=(3\pm1)\ 10^{-2}\ s/\mu m$ (Fig. 2H). This suggests that both vesicles and the cytoplasmic F-actin

display an active diffusive motion, with a component that depends on cytoplasmic streaming, and a component that does not.

To further assess the influence of flows on cytoplasmic dynamics we first attempted to eliminate kinesin-1, the motor responsible for flows (13, 34). However, the morphology of the actin mesh was massively disturbed in oocytes lacking kinesin, and large aggregations of F-actin were observed instead (Fig. S3A,B) (35). However, it is known that the mesh is present in oocytes that lack microtubules (15), a fact that we used to test our hypothesis in oocytes obtained from females fed with the microtubule depolymerizing drug colchicine (Fig. 3A,B and Fig. S3C,D). In oocytes without microtubules – and consequently without flows - the ballistic movement of cytoplasmic F-actin and vesicles was completely abrogated, while a random diffusive motion was still detected (Fig. 3C and Movie S2). Remarkably, the experimental values found in the absence of flow for $D_{act,nf}$ = (2.8±1) 10^{-3} $\mu m^2/s$ and $D_{ves,nf}$ = (1.4±0.5) 10^{-3} $\mu m^2/s$ (where nf stands for "no flow") are in excellent agreement with the values $D_{ves,0}$ and $D_{act,0}$ obtained as extrapolation to zero-flow conditions of the experimental data in the presence of flow (Fig. 2H).

A final interesting correlation, valid also when microtubules are depolymerized, is that the diffusivity of actin is always faster than the diffusivity of the vesicles, and can be described as $D_{act} \simeq 2D_{ves}$ (Fig. 2G,H and Fig. 3C). The active diffusion of vesicles is seemingly locked to the dynamics of the actin mesh, suggesting that the active diffusive motion of the vesicles might originate from actin activity. Our results qualitatively agree with a recent model (19) in which vesicles are caged in the cytoskeleton and the latter act as an actively rearranging harmonic trap for the former. Unfortunately, the rearrangement dynamics of the actin network in (19) is not explicitly described, as its effect on a tracer particle is described as an effective random force. However, as long as the tracer particle is larger than the actin mesh size, the model predicts that the particle mean square displacement is inversely proportional to its size. In general, we can thus expect in our experiments that a vesicle of size d_{ves} larger than the actin mesh size l_{act} will have an effective diffusion coefficient $D_{eff} < D_{act}$, the limit case being $d_{ves} \simeq l_{act}$ for which $D_{eff} \simeq D_{act}$. With the naïve assumption $D_{eff} \simeq D_{act}*(l_{act}/d_{ves})$ we can expect that if $D_{act} \simeq 2D_{ves}$, then the actin mesh size in our experiments is $l_{act} \simeq d_{ves}/2$. Since in our images the vesicles are large and clearly visible, we evaluated their diameter under different experimental conditions. For both control and colchicine treated oocytes we find the same result d_{ves} = (1.0 ± 0.2) μm. As for the characteristic length-scale l_{act} for the actin mesh, we calculated the spatial autocorrelation function of the image intensity (Fig. S3E). Fitting to an exponentially decaying function provided the characteristic length-scale

l_{act} = (0.42 ± 0.09) μm and l_{act} = (0.55 ± 0.05) μm, for control and colchicine-treated oocytes, respectively. We thus obtained l_{act}/d_{ves} = 0.42 ± 0.03 (control) and l_{act}/d_{ves} = 0.55 ± 0.12 (colchicine) that are both compatible with the expected value D_{ves} / D_{act} ~1/2 found from the dynamics. These results point to the active diffusion of vesicles being due to the non-equilibrium active dynamics of the underlying actin mesh, a hypothesis that will be further scrutinized in the following.

The observed correlation between vesicles and actin dynamics is compatible with recent findings obtained from mouse oocytes, in which vesicles are transported throughout the cell by myosin walking along a F-actin mesh, whose nodes are occupied by vesicles as well (16, 33). An important difference between mammalian and *Drosophila* oocytes is that at the time the actin mesh is present, microtubules are engaged in forming the meiotic spindle in mammals, while in *Drosophila* oocytes, microtubules display an organization similar to a cell in interphase, active in microtubule transport. Despite these differences, our results suggest that the dynamic link between vesicles and actin, and the molecular mechanism responsible for it, are conserved, and survive the presence of microtubule-dependent streaming flows in *Drosophila*. This is further supported by the fact that the mouse actin mesh depends on the corporative activity of the actin nucleators Spire and Formin2 (36)

Cytoplasmic motility is driven by active processes

The major energy source in cells is ATP, and ATP-dependent random force fluctuations have been observed in prokaryotes and eukaroytes (8, 10, 11). The observed pattern of cytoplasmic motility in our cells prompted us to experimentally test the active nature of the diffusion-like motion. Therefore, we depleted ATP by treating dissected ovaries with sodium azide and 2-D-deoxyglucose shortly before image acquisition. After acute treatment the actin mesh remains intact in about half the cells and ATP depletion leads to an immediate reduction in all cytoplasmic motion. Both, persistent and diffusive behavior of vesicles and actin, are substantially abrogated (Fig. 3D,E, Fig. S3F-H and Movie S3).

A reliable quantification with DDM of the residual dynamics was difficult due to presence of a marked plastic deformation of the whole cell (Movie S3). Nevertheless, in ATP-depleted cells, in which this effect was less pronounced, the dynamics of both vesicles and actin could be successfully measured. This was achieved by adopting an advection-diffusion model, like the one described by Eq. (1), where now the advection velocity is assumed to be the same for all particles and, corresponding to the drift velocity, is not significant from a physical point of view. In ATP depleted cells, we find a residual diffusive-like motion, existing on top of the constant drift (Fig. 3F). The average values of the diffusivities associated with vesicles and

actin motion are $D_{ves,ATPd}$ = (1±0.5) 10^{-4} $\mu m^2/s$ and $D_{act,ATPd}$ = (1.4±0.8) 10^{-4} $\mu m^2/s$, respectively (here ATPd stands for "ATP-depleted"). These values are about 30 times smaller than the ones obtained in control cells.

Thus, ballistic and diffusive motions displayed by vesicles and cytoplasmic F-actin are strongly ATP-dependent. Since the persistent motion relies entirely on microtubule based processes (transport and advection), we then asked what the source of the active diffusion is.

Cytoplasmic F-actin is the major source of active diffusion

F-actin, together with myosins, is the source of active diffusion processes in various cell types (8, 23-25). Therefore, we decided to test whether the cytoplasmic actin network might be driving the diffusive behavior of vesicles in the oocyte. We first tested whether active force fluctuations depend on the level of F-actin in the cell. For this purpose, we studied the motion of both F-actin and vesicles in oocytes that overexpress the actin nucleator Spire. SpireB is the only one, out of four isoforms, to be able to rescue all aspects of *spire* mutants (26). Nevertheless, the effect of SpireB overexpression in wild type cells has never been studied. Driving SpireB, under the control of the germline specific Gal4 driver *nanos*-Gal4 (*nos*-Gal4) and the presence of endogenous Spire, results in a dramatic reduction of st9 flows, stratification of the oocyte and complete female sterility (Movie S4 and data not shown). This over-expression of SpireB also induces the formation of actin filaments in the cytoplasm of nurse cells (Fig. 4A,B and Fig. S4)(26). To verify that F-actin concentrations are also higher in the oocyte, we stained for F-actin in fixed cells, using TRITC-labeled phalloidin, and measured the mean fluorescence intensities. We found that the fluorescence intensities in SpireB overexpressing cells are increased by about 1.4-fold compared to controls, showing that the overall amount of actin filaments is increased (Fig. S4B). We also measured the mean distance between bright actin filaments as an indicator of the mesh size in the same cells and found no apparent difference between the genotypes (data not shown).

We then analyzed how the overexpression of SpireB and the higher content of actin filaments affect cytoplasmic motility. The most striking effect we found is the strong reduction of the cytoplasmic streaming. The ballistic contribution to the dynamics is so small that for some cells it cannot be reliably measured. Overall, DIC-DDM and Con-DDM analyses provide the following upper bound for the streaming speed: $v_{ves,SpireOE} \simeq v_{act,SpireOE} < 2$ nm/s (where SpireOE stands for Spire "over-expression"), a value that is at least one order of magnitude smaller than the typical streaming speed obtained for the control cells. For these Spire over-expressing oocytes, the dynamics are thus substantially diffusive-like, with

diffusivities: $D_{ves,SpireOE}$ = (1.4±0.5) 10^{-3} $\mu m^2/s$ and $D_{act,SpireOE}$ = (2.3±0.8) 10^{-3} $\mu m^2/s$. These values are similar to the ones obtained when microtubules are depolymerized, and flows are abrogated. However, in the present case we were not able to study reliably the connection between the dynamics and the spatial correlation properties of actin and vesicles, since SpireB over-expression causes a marked cell-to-cell variability in the vesicle size that prevents a meaningful sizing with the available data. Despite this, our data confirm that both flows and active diffusion depend on a well-regulated concentration of cytoplasmic F-actin, and further supports a close link between the motion of cytoplasmic F-actin and vesicles.

It is important to note that by over-expressing SpireB in a *spire* mutant background, the mesh is less sensitive to Latrunculin A (LatA) treatment (26). LatA is a G-actin sequestering substance that not only inhibits *de novo* formation of actin filaments, but also causes the depolymerization of dynamic actin filaments. In wild type oocytes, LatA treatment leads to the destruction of the actin mesh (15), even within minutes of exposure to the drug (15, 37). However, in oocytes where SpireB expression is driven by an artificial promotor (as in our experiment), LatA treatment remains without any effect (26). Thus, in SpireB over-expressing oocytes, the aberrant mesh appears to have more, but less dynamic, filaments. This suggests that actin turnover contributes to active diffusion, and it might explain why the diffusive motion of F-actin and vesicles drops in SpireB over-expressing oocytes. Of note, the ectopic expression of Capuccino, a formin jointly working with Spire in forming the actin mesh, also increases the number of actin filaments but does not affect cytoplasmic flows (as measured by PIV) (38). It is not known why expression of those actin nucleators has a different impact on cytoplasmic flows. However, these observations suggest that a higher concentration of F-actin in the cytoplasm is not enough to substantially inhibit flows.

We finally asked how the motion of vesicles changes in oocytes lacking cytoplasmic F-actin. *spire* mutant oocytes do not show any obvious defects in cortical actin organization, but lack the cytoplasmic F-actin network and display premature fast streaming (Fig. 4C,D and Movie S4) (15, 29, 34, 39). DIC-DDM analysis revealed flow velocities in *spire* mutant oocytes nearly 5 fold faster than in control oocytes (v_{ves}=(150±70) nm/s and (26)) making the detection of any superimposed diffusive motion difficult (see also Movie S4). To yet be able to measure diffusivity, we eliminated flows by treating dissected *spire* mutant oocytes with colchicine. In oocytes lacking cytoplasmic actin and microtubules we measure a residual, slow, diffusive-like motion of the vesicles, with an effective diffusion coefficient $D_{ves,spire}$=(6±2) 10^{-4} $\mu m^2/s$ (see also Movie S4). This value is about five times smaller than the value measured in control cells and is twice the thermal diffusion coefficient D_{TH}=3.1 10^{-4} $\mu m^2/s$,

estimated by using the viscosity value obtained in (14). The diffusivity $D_{ves,spire}$=(6±2) 10^{-4} m^2/s in colchicine treated spire mutants is about six times larger than the diffusivity $D_{ves,ATPd}$ = (1±0.5) 10^{-4} $\mu m^2/s$ measured in ATP depleted cells. This difference might be due either to the presence of microtubule and actin independent residual active processes or by changes in the cytoplasmic viscosity due to the lack of both microtubules and F-actin.

Concluding remarks

In the *Drosophila* oocyte, streaming promotes the mixing and transport of cytoplasmic components (13, 40) and is required for essential events for embryogenesis, such as the localization of mitochondria (41) and of the developmental determinant *nanos* mRNA (5, 42). Not surprisingly, streaming is more efficient than thermal diffusion in transporting large organelles (e.g. vesicles) for long distances (43). However, recent studies in mouse oocytes, which lack microtubule-dependent streaming, outlined the important role of active diffusion mechanisms, seemingly dependent on a novel cytoplasmic F-actin cytoskeleton (far from the cortex and cortical F-actin) (10, 23, 24, 44). It is thus worth assessing whether diffusion still plays a role in the presence of streaming and, if that is the case, what is the interplay between directed and random motion. In this work, we have developed a robust methodology allowing, for the first time, to separate the persistent motion - due to cytoplasmic flow - from the random motion due to diffusion inside a cell. We have also explored how the cytoplasmic F-actin cytoskeleton affects particle dynamics, a question that is largely unknown. In particular, we used Differential Dynamic Microscopy with different contrast mechanisms (DIC and confocal imaging) in combination with genetic and chemical manipulations of the cytoskeletons in the oocyte. We found that both vesicles and cytoplasmic actin filaments move in a persistent manner by advection, mainly as a result of microtubule-dependent flows. In addition, they display a non-thermal, active diffusion that is dependent on cytoplasmic but not cortical actin. In fact, we speculate that cytoplasmic F-actin is the major driving force behind active diffusion in the *Drosophila* oocyte. We also found that active diffusion is reduced in oocytes without microtubules, which suggests that microtubules are important, not only for active transport of cargoes and cytoplasmic streaming, but also for active diffusion. This may constitute a difference with the mouse oocytes, as well as with various cultured cells where active fluctuations have been measured (8, 25, 45). However, the involvement of microtubules in the cytoplasmic motion of cultured cells was not investigated in detail in these studies.

Our study sheds light on the link between the motion of different cytoplasmic components, in particular between large vesicles and cytoplasmic F-actin which are found to exhibit the same advection-diffusion dynamics. This link is robust upon perturbation of cytoplasmic

streaming, and our findings suggest that cytoplasmic F-actin, a dense non-equilibrium fluctuating mesh, is the source of active diffusion for the vesicles. In the future, this link will need to be studied in more depth, for instance by performing a more detailed analysis of the correlation between the size of the actin mesh and of the vesicles that we found here. For instance, it would be of interest to study such correlation as a function of the vesicle size.

References

1. Luby-Phelps K, Castle PE, Taylor DL, & Lanni F (1987) Hindered diffusion of inert tracer particles in the cytoplasm of mouse 3T3 cells. *Proc Natl Acad Sci U S A* 84(14):4910-4913.
2. Phillips R, Kondev J, Theriot J, & Garcia H (2012) Physical Biology of the Cell (2nd Edition). *Garland Science*.
3. Corti B (1774) Osservazioni microscopiche sulla tremella e sulla circolazione del fluido in una pianta acquajuola. *(Appresso Giuseppe Rocchi, Lucca, Italy).*
4. Shimmen T & Yokota E (2004) Cytoplasmic streaming in plants. *Curr Opin Cell Biol* 16(1):68-72.
5. Quinlan ME (2016) Cytoplasmic Streaming in the Drosophila Oocyte. *Annu Rev Cell Dev Biol* 32:173-195.
6. Goldstein RE, Tuval I, & van de Meent JW (2008) Microfluidics of cytoplasmic streaming and its implications for intracellular transport. *Proc Natl Acad Sci U S A* 105(10):3663-3667.
7. Brangwynne CP, MacKintosh FC, & Weitz DA (2007) Force fluctuations and polymerization dynamics of intracellular microtubules. *Proc Natl Acad Sci U S A* 104(41):16128-16133.
8. Guo M*, et al.* (2014) Probing the stochastic, motor-driven properties of the cytoplasm using force spectrum microscopy. *Cell* 158(4):822-832.
9. Hoffman BD, Massiera G, Van Citters KM, & Crocker JC (2006) The consensus mechanics of cultured mammalian cells. *Proc Natl Acad Sci U S A* 103(27):10259-10264.
10. Parry BR*, et al.* (2014) The bacterial cytoplasm has glass-like properties and is fluidized by metabolic activity. *Cell* 156(1-2):183-194.
11. Weber SC, Spakowitz AJ, & Theriot JA (2012) Nonthermal ATP-dependent fluctuations contribute to the in vivo motion of chromosomal loci. *Proc Natl Acad Sci U S A* 109(19):7338-7343.
12. Brendza RP, Serbus LR, Duffy JB, & Saxton WM (2000) A function for Kinesin I in the posterior transport of *oskar* mRNA and Staufen protein. *Science* 289(5487):2120-2122.
13. Palacios IM & St Johnston D (2002) Kinesin light chain-independent function of the Kinesin heavy chain in cytoplasmic streaming and posterior localisation in the Drosophila oocyte. *Development* 129(23):5473-5485.
14. Ganguly S, Williams LS, Palacios IM, & Goldstein RE (2012) Cytoplasmic streaming in Drosophila oocytes varies with kinesin activity and correlates with the microtubule cytoskeleton architecture. *Proc Natl Acad Sci U S A* 109(38):15109-15114.
15. Dahlgaard K, Raposo AA, Niccoli T, & St Johnston D (2007) Capu and Spire assemble a cytoplasmic actin mesh that maintains microtubule organization in the Drosophila Oocyte. *Dev Cell* 13(4):539-553.
16. Schuh M (2011) An actin-dependent mechanism for long-range vesicle transport. *Nat Cell Biol* 13(12):1431-1436.
17. Cerbino R & Trappe V (2008) Differential dynamic microscopy: probing wave vector dependent dynamics with a microscope. *Phys Rev Lett* 100(18):188102.

18. Giavazzi F & Cerbino R (2014) Digital Fourier Microscopy for Soft Matter Dynamics. *J. Opt* 16.
19. Fodor E*, et al.* (2015) Active-driven fluctuations in living cells. *EPL (Europhysics Letters)* 110(4):48005.
20. Kugler J-M & Lasko P (2009) Localization, anchoring and translational control of oskar, gurken, bicoid and nanos mRNA during Drosophila oogenesis. *Fly* 3:15-28.
21. Cerbino R & Trappe V (2008) Differential dynamic microscopy: Probing wavevector-dependent dynamics with a microscope. *Phys. Rev. Lett* 100(188102).
22. Berne BJ & Pecora R (1976) Dynamic Light Scattering: With Applications to Chemistry, Biology, and Physics.
23. Almonacid M*, et al.* (2015) Active diffusion positions the nucleus in mouse oocytes. *Nat Cell Biol* 17(4):470-479.
24. Ahmed WW*, et al.* (2016) Active mechanics reveal molecular-scale force kinetics in living oocytes. *arXiv:1510.08299v2*.
25. Fakhri N*, et al.* (2014) High-resolution mapping of intracellular fluctuations using carbon nanotubes. *Science* 344(6187):1031-1035.
26. Quinlan ME (2013) Direct interaction between two actin nucleators is required in Drosophila oogenesis. *Development* 140(21):4417-4425.
27. Manseau LJ & Schupbach T (1989) cappuccino and spire: two unique maternal-effect loci required for both the anteroposterior and dorsoventral patterns of the Drosophila embryo. *Genes Dev* 3(9):1437-1452.
28. Wu JQ & Pollard TD (2005) Counting cytokinesis proteins globally and locally in fission yeast. *Science* 310(5746):310-314.
29. Wang Y & Riechmann V (2008) Microtubule anchoring by cortical actin bundles prevents streaming of the oocyte cytoplasm. *Mech Dev* 125(1-2):142-152.
30. Burkel BM, von Dassow G, & Bement WM (2007) Versatile fluorescent probes for actin filaments based on the actin-binding domain of utrophin. *Cell Motil Cytoskeleton* 64(11):822-832.
31. Rauzi M, Lenne PF, & Lecuit T (2010) Planar polarized actomyosin contractile flows control epithelial junction remodelling. *Nature* 468(7327):1110-1114.
32. Lu PJ*, et al.* (2012) Characterizing concentrated, multiply scattering, and actively driven fluorescent systems with confocal differential dynamic microscopy. *Phys Rev Lett* 108(21):218103.
33. Holubcova Z, Howard G, & Schuh M (2013) Vesicles modulate an actin network for asymmetric spindle positioning. *Nat Cell Biol* 15(8):937-947.
34. Serbus LR, Cha BJ, Theurkauf WE, & Saxton WM (2005) Dynein and the actin cytoskeleton control kinesin-driven cytoplasmic streaming in Drosophila oocytes. *Development* 132(16):3743-3752.
35. Williams LS, Ganguly S, Loiseau P, Ng BF, & Palacios IM (2014) The auto-inhibitory domain and ATP-independent microtubule-binding region of Kinesin heavy chain are major functional domains for transport in the Drosophila germline. *Development* 141(1):176-186.
36. Pfender S, Kuznetsov V, Pleiser S, Kerkhoff E, & Schuh M (2011) Spire-type actin nucleators cooperate with Formin-2 to drive asymmetric oocyte division. *Curr Biol* 21(11):955-960.
37. Manseau L, Calley J, & Phan H (1996) Profilin is required for posterior patterning of the Drosophila oocyte. *Development* 122(7):2109-2116.
38. Bor B, Bois JS, & Quinlan ME (2015) Regulation of the formin Cappuccino is critical for polarity of Drosophila oocytes. *Cytoskeleton (Hoboken)* 72(1):1-15.
39. Theurkauf WE (1994) Premature microtubule-dependent cytoplasmic streaming in cappuccino and spire mutant oocytes. *Science* 265(5181):2093-2096.
40. Glotzer JB, Saffrich R, Glotzer M, & Ephrussi A (1997) Cytoplasmic flows localize injected oskar RNA in Drosophila oocytes. *Curr Biol* 7(5):326-337.
41. Hurd TR*, et al.* (2016) Long Oskar Controls Mitochondrial Inheritance in Drosophila melanogaster. *Dev Cell* 39(5):560-571.

42. Forrest KM & Gavis ER (2003) Live imaging of endogenous RNA reveals a diffusion and entrapment mechanism for nanos mRNA localization in Drosophila. *Curr Biol* 13(14):1159-1168.
43. Goldstein RE (2016) Batchelor Prize Lecture. Fluid dynamics at the scale of the cell. *J. Fluid Mech.* 807:1-39.
44. Brangwynne CP, Koenderink GH, MacKintosh FC, & Weitz DA (2009) Intracellular transport by active diffusion. *Trends Cell Biol* 19(9):423-427.
45. Katrukha A*, et al.* (2016) Probing cytoskeletal modulation of passive and active intracellular dynamics using nanobody-functionalized quantum dots. *bioRxiv*.
46. Brendza KM, Rose DJ, Gilbert SP, & Saxton WM (1999) Lethal kinesin mutations reveal amino acids important for ATPase activation and structural coupling. *J Biol Chem* 274(44):31506-31514.
47. Giavazzi F, Brogioli D, Trappe V, Bellini T, & Cerbino R (2009) Scattering information obtained by optical microscopy: differential dynamic microscopy and beyond. *Phys Rev E Stat Nonlin Soft Matter Phys* 80(3 Pt 1):031403.
48. Bacallao R, Garfinkel A, Monke S, Zampighi G, & Mandel LJ (1994) ATP depletion: a novel method to study junctional properties in epithelial tissues. I. Rearrangement of the actin cytoskeleton. *J Cell Sci* 107 (Pt 12):3301-3313.

MATERIALS AND METHODS

Fly stocks and genetics:

If not stated otherwise, all flies where kept on standard cornmeal agar at room temperature. Fly stocks used in this study where: *w*[1118], *w*;*CyO/Sco*;P{*sqh*-UTRN.GFP}/TM6B,*Hu*[1],*Tb*[1] (31), *w*;*CyO/Bl*;P{UASp-SpirB.td.Tomato} (gift from M. Quinlan), w;;P{GAL4::VP16-*nos*.UTR} (BL4937), *w*;FRTG13,*Khc*[27]*CyO* (46), *w*;*spir*[1]/CyO;P{*sqh*-UTRN.GFP}/TM6B,*Hu*[1],*Tb*[1] (BL5113), *w*;Df(2L)Exel6046/*CyO* (BL7528), w[*];P{UASp-GFP.Act5C}3 (BL9257) and w[*];P{UASp-Act5C.mRFP}38 (BL24779).

All UAS/Gal4 crosses were performed at 25˚C, germ line clones where induce using the FLP;FRT *ovoD* system. The stock *w*;*CyO/Sco*; *nos*-Gal4.VP16,*sqh*-UTRN.GFP/TM6B was generated by the recombination of the respective chromosome (this study).

Actin mesh staining in fixed samples:

Ovaries where dissected and fixed in 10% methanol free formaldehyde in PBS, containing 0.1% Tween-20 (PBT0.1), for a maximum of 10 min. The fixed cells were washed 4x in PBT0.1 and stained with 1µM TRITC coupled phalloidin (in PBT0.1, Sigma-Aldrich) over night at 4˚C. The stained samples where washed 4x in PBT0.1 and mounted in Vectashield mounting medium (Vectorlabs). Images were acquired on a Leica SP5 inverted confocal microscope, using a 40x/1.3 Oil DIC Plan-Neolfuar or a 100x/1.4 Oil DIC objective. Images were taken within 24h after staining.

Live imaging of the actin mesh:

Ovaries of *sqh*-UTRN.GFP flies were dissected in a drop of halocarbon oil (Voltalef 10S, VWR) on a glass coverslip and single egg chambers were separated using fine tungsten needles. Images were acquired on a Leica SP5 inverted confocal microscope, using a 40x/1.3 Oil DIC Plan-Neolfuar or a 100x/1.4 Oil DIC objective.

For high-resolution image series, a single plane from the middle of the oocyte was imaged at a scan speed of 100Hz and an image resolution of 1024x1024 pixels (corresponding to one image every 10.4 s).

For DDM analyses images where taken at a scan speed of 400Hz and a resolution of 1024 x 512 pixels, corresponding to one image every 1.29 s. The pinhole diameter was set to a corresponding thickness of the image plain of about 1.39 µm. The cells were illuminated by 488 nm and 561 nm laser light and emission light was collected simultaneously using a hybrid detector at 500-550 nm (GFP), a conventional photon multiplier at 560-650 nm (vesicle auto-fluorescence) and a transmitted light detector with DIC filter set.

Drug treatment:

Depolymerization of microtubules was achieved by either feeding (Figure 3) or treatment of dissected egg chambers. For the feeding experiment, 200µg/ml colchicine were diluted in yeast paste and fed to female flies for 16h at 25˚C. For short-term treatment, flies were fattened overnight, ovaries dissected in dissection medium (1x Schneider's medium + 2% DMSO) and treated in 20µg/ml colchicine in dissection medium for 5 min at room temperature (Fig. 4). Ovaries were washed once in a drop of dissection medium and dissected in halocarbon oil. Imaging was perfomred as described above. ATP was depleted by treating dissected ovaries in 0.4 mM NaN3 and 2 mM 2-Deoxy-D-glucose in dissection medium for 5.5 minutes at room temperature (Fig. 3 and Fig. 3F-H). Ovaries were washed in a drop of dissection medium and further dissected and imaged in a drop of halocarbon oil.

Differential Dynamic Microscopy (DDM)

DDM analysis was performed by using both DIC imaging (DIC-DDM) and confocal imaging (Con-DDM). While Con-DDM was previously demonstrated with densely packed bacteria and colloids (32), both techniques are employed here for the first time to probe the cell interior dynamics. Time lapse movies acquired at a fixed frame rate with either imaging mode are treated in the same way. Reciprocal space information is extracted from the analysis of the N intensity frames of the video $i_n(\boldsymbol{x}) = i(\boldsymbol{x}, n\delta t)$ acquired at times $n\delta t$ (n=1,…,N) by calculating their spatial Fourier transform $I_n(\boldsymbol{q}) = \int e^{j\boldsymbol{q}\cdot\boldsymbol{x}} i_n(\boldsymbol{x}) d^2x$. Here j is the imaginary unit, δt is the inverse frame rate of the video acquisition, $\boldsymbol{x} = (x, y)$ are the real space coordinates and $\boldsymbol{q} = (q_x, q_y)$ are the reciprocal space coordinates. DDM analysis is based on calculating the *image structure function* defined as

$$d(\boldsymbol{q}, \Delta t) = \langle |I_{n+m}(\boldsymbol{q}) - I_n(\boldsymbol{q})|^2 \rangle_n$$

where the average $\langle \dots \rangle_n$is made over image pairs that are separated by the same time delay $\Delta t = n\delta t$ over the entire stack. The azimuthal average

$$d(q, \Delta t) = \langle d(\boldsymbol{q}, \Delta t) \rangle_{q=\sqrt{q_x^2+q_y^2}}$$

is also typically performed whenever the structure and the dynamics of the sample are isotropic and spatially homogeneous in the image plane, as in the present study. Once the image structure function is calculated, it can be fitted to the following theoretically expected behavior

$$d(q, \Delta t) = A(q)[1 - f(q, \Delta t)] + B(q).$$

Here B(q) is a background term due to the detection noise, A(q) is an amplitude term that contains information about the imaging mode used and the distribution of individual entities

in the image, and $f(q,\Delta t)$ is the so-called *intermediate scattering function*, which encodes the information about the sample dynamics (17, 47). For instance, diffusive motion with diffusion coefficient D is characterized by $f(q,\Delta t) = e^{-Dq^2\Delta t}$ and ballistic motion with constant velocity $\boldsymbol{v_0}$ is described by $f(\boldsymbol{q},\Delta t) = e^{-j\boldsymbol{v_0}\cdot\boldsymbol{q}\Delta t}$ (18)

A case of interest for the present study is the one of a collection of particles moving via a combination of ballistic and Brownian motion, the first being characterized by a constant velocity **v** drawn from a prescribed distribution p(**v**), the second by a diffusion coefficient D. In this case the intermediate scattering function reads

$$f(\boldsymbol{q},\Delta t) = e^{-Dq^2\Delta t}\int p(\boldsymbol{v})e^{-j\boldsymbol{v_0}\cdot\boldsymbol{q}\Delta t}d^3\boldsymbol{v} = e^{-Dq^2\Delta t}P(\boldsymbol{q}\Delta t)$$

where P is the three-dimensional Fourier transform of p. If the velocity distribution is isotropic, it can be written in terms of the speed distribution $p_{s,3D}(v)$

$$p(\boldsymbol{v}) = \frac{1}{4\pi|\boldsymbol{v}|^2}p_{s,3D}(|\boldsymbol{v}|)$$

that we assume to be in the form of a Shultz distribution

$$p_{s,3D}(v) = \frac{v^Z}{Z!}\left(\frac{Z+1}{\bar{v}}\right)e^{-\frac{v}{\bar{v}}(Z+1)}.$$

Here Z is a shape parameter (set to 2 in our case) and $\bar{v}$ is the average speed:

$$\bar{v} = \int vp_{s,3D}(v)dv.$$

If a 2D projection of the motion is considered, the speed distribution reads

$$p_{s,2D}(v) = \int p(\boldsymbol{v})\delta\left(v - \sqrt{v_x + v_y}\right)d^3\boldsymbol{v}.$$

where δ is the Dirac delta function. This is the quantity that is typically measured with PIV. It is important to note that, in general, the mean value of the 2D projected velocity field:

$$\bar{u} = \int vp_{s,2D}(v)dv$$

does not coincide with $\bar{v}$. For example, in our case, it can be shown that $\bar{u} = 0.566\bar{v}$.

The accessible q-range for DDM analysis is given, in principle by $[2\pi/L, \pi/a]$ where L is the size of the considered region of interest and a is the effective pixel size (typically L=33 μm, a=0.13 μm). In practice, this range can be significantly reduced. This can be due, at low q, to the presence of very slow dynamics that cannot be fully captured during the finite duration of the image acquisition and, at high q, mainly to the loss of signal due to the microscope transfer function (that depress higher spatial frequencies in the image) and to the presence of dynamics that are too fast to be sampled with the experimental frame rate. Overall, in the majority of the experiments presented in this work, the effective q-range roughly

corresponds to [2, 20] μm^{-1}. In the direct space, this corresponds to considering density fluctuations on length scales comprised approximately between 0.3 μm and 3 μm.

ACKNOWLEDGEMENTS

We thank Dr. Margot E. Quinlan for comments and for reagents, and M. Wayland for assistance with imaging. MD and IMP were supported by the BBSRC, the Department of Zoology (Cambridge), and the University of Cambridge. FG and RC acknowledge funding by the Italian Ministry of Education and Research, Futuro in Ricerca Project ANISOFT (RBFR125H0M) and by Fondazione CARIPLO-Regione Lombardia Project Light for Life (2016-0998).

AUTHOR CONTRIBUTIONS

MD, FG, IP and RC designed experiments, analyzed the data, discussed results and wrote the manuscript. MD and FG performed experiments.

Figures

Drechsler et al. Figure 1

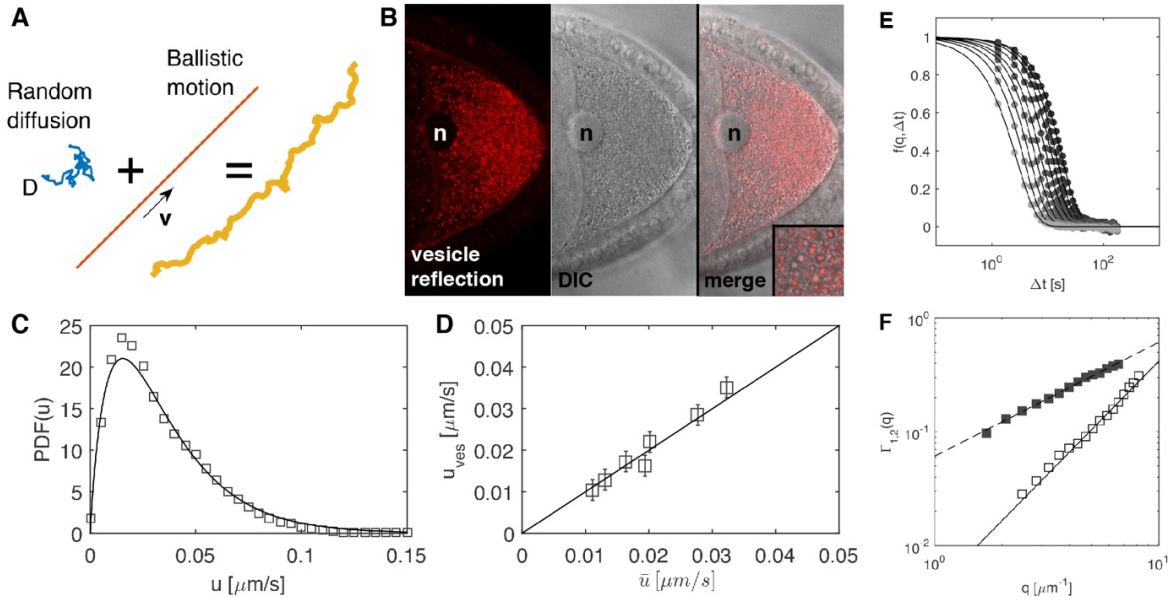

Figure 1. Movement of cytoplasmic vesicles consists of persistent and diffusive motions. ***(A)*** Sketch depicting the complex motion of particles in the cytoplasm. Each particle (e.g. an organelle, a protein or protein complex) moves by random diffusion, described by a characteristic diffusion coefficient *D* (blue). This random motion can be superimposed to a persistent, ballistic motion, described by a characteristic velocity ***v*** (red line). Both together result in the persistent, erratic movement of tracer particles observed in the cell (orange). ***(B)*** Still frame of a movie showing reflection of endogenous vesicles in the *Drosophila* stage 9 oocyte, imaged by confocal microscopy (left panel), and the same vesicles imaged by DIC microscopy (middle panel). The merge of both signals reveals that the reflective signal co-localizes very well with the center of vesicles (right panel, inset). The nucleus (n) is visible at the anterior side of the cell. ***(C)*** Probability distribution function (PDF) of the 2D streaming speed in a single control cell, as obtained from PIV analysis (open boxes) and as reconstructed from DIC-DDM analysis (solid line). ***(D)*** Comparison of 2D mean streaming speeds obtained by DIC-DDM (u_{ves}) and PIV ($\bar{u}$) for each cell tested. The values are in very good agreement (the continuous line represents $u_{ves} = \bar{u}$), validating DIC-DDM as a reliable method for the quantification of cytoplasmic flows. ***(E)*** Intermediate scattering functions $f(q, \Delta t)$ obtained from DIC-DMM analysis on the same cell shown in panel (C) for different wave vectors *q* in the range 1.8 μm^{-1} <q< 8 μm^{-1}. Continuous lines are best fits to Eq. (1) ***(F)*** Decorrelation rates $\Gamma_1(q)$ (solid black boxes) and $\Gamma_2(q)$ (open boxes) obtained from the fit of the intermediate scattering functions represented in panel (E) plotted against the wave vector *q*. $\Gamma_1(q)$, which accounts for the ballistic contribution to the motion of the vesicles, exhibits a

linear scaling $\Gamma_1(q) = v_{ves} q$ (dashed line), while $\Gamma_2(q)$, which describes a diffusive-like relaxation process, is well fitted to a quadratic law $\Gamma_2(q) = D_{ves} q^2$ (continuous line).

Drechsler et al. Figure 2

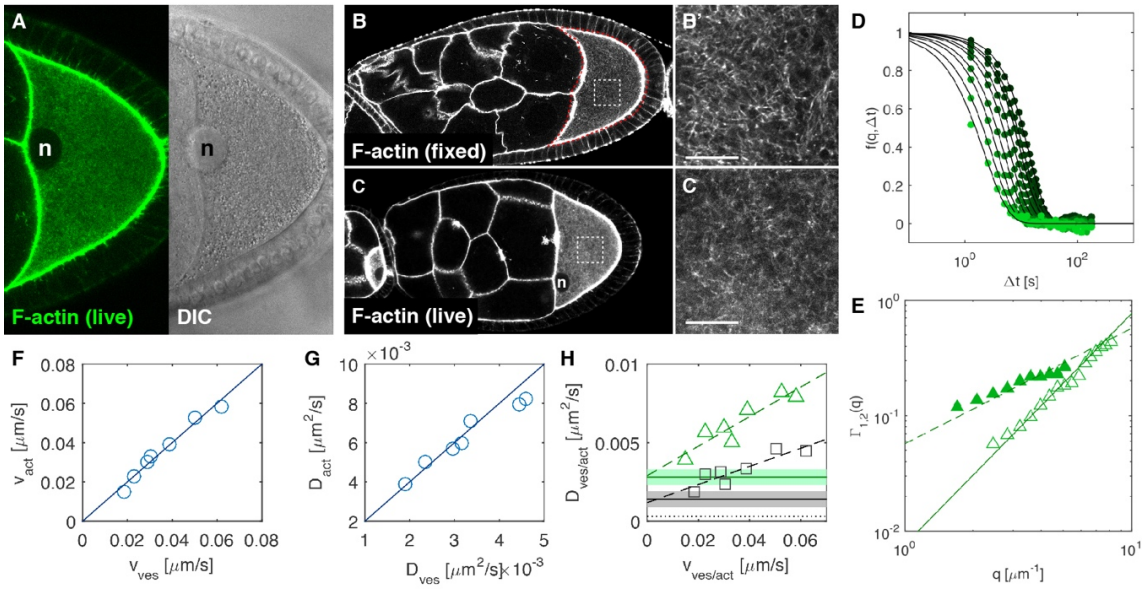

Figure 2. The motion of cytoplasmic F-actin directly correlates with the motion of vesicles. ***(A)*** Left panel: Still frame from a movie, showing expression of the F-actin binding protein UTRN.GFP (*sqh*-UTRN.GFP). Both the cortex and the cytoplasm of the stage 9 oocyte are enriched in F-actin. The nucleus (n) is visible at the anterior side of the oocyte. Right panel: DIC image if the same oocyte. ***(B)*** Distribution of F-actin (stained with TRITC-phalloidin) in a fixed stage 9 egg chamber. F-actin can be found along the cortex of all cells of the egg chamber. Within the oocyte (red outlined cell), actin filaments also traverse the whole cytoplasm. ***(B')*** High magnification image of cytoplasmic actin filaments in the oocyte (white boxed area in B). The cytoplasmic actin network consists of short filaments and actin rich dots or foci. Scale bar represents 10 μm. ***(C)*** Distribution of F-actin in a living egg chamber, ubiquitously expressing UTRN.GFP (*sqh*-UTRN.GFP). Compared to fixed samples (in B), UTRN.GFP labels the same structures as phalloidin. ***(C')*** High magnification image of cytoplasmic actin filaments in a living oocyte (white boxed region in C). Filaments and foci are labeled by the UTRN.GFP probe. Scale bar represents 10μm. ***(D)*** Intermediate scattering functions $f(q,\Delta t)$ obtained from Con-DMM analysis (on the same cell considered in Figs. 1C, 1E and 1F) for different wave vectors *q* in the range 2 μm^{-1} <q< 8 μm^{-1}. Continuous lines are best fit to Eq. (1) ***(E)*** Decorrelation rates $\Gamma_1(q)$ (solid green triangles) and $\Gamma_2(q)$ (open green triangles). The dashed line is the best fitting curve of $\Gamma_1(q)$ to a linear function $\Gamma_1(q) = v_{act} q$, while the continuous line is obtained from the fit of $\Gamma_2(q)$ to a quadratic function $\Gamma_2(q) = D_{act} q^2$ ***(F)*** Mean speed for F-actin (v_{act}), plotted against the mean speed obtained for vesicles (v_{ves}) with each data point corresponding to one cell. The continuous line represents v_{act} = v_{ves}. The close correspondence between v_{act} and v_{ves} indicates a physical coupling

between the ballistic component of the motion of vesicles and actin filaments. ***(G)*** Diffusion coefficient obtained for F-actin (D_{act}) plotted against the diffusion coefficient of vesicles (D_{ves}). The strong linear correlation suggests the presence of a common mechanism driving the diffusive relaxation of both structures. Each data point represents the diffusion coefficient determined for one cell, the continuous line corresponds to $D_{act} = 2\ D_{ves}$. ***(H)*** Diffusion coefficients (D) of F-actin (green triangles, D_{act}) and vesicles (black boxes, D_{ves}) as a function of the respective mean advection speed v_{act} and v_{ves}. The dependence of the diffusivity of both structures on their respective speeds indicates that the physical mechanisms driving advection also contribute to their diffusion. While the persistent velocities (v) of F-actin and vesicles are rather similar within each cell, the diffusivity of actin D_{act} is consistently higher (by about a factor of 2, see also panel G) compared to the diffusivity of vesicles D_{ves}. Horizontal solid lines represent the diffusivities $D_{ves,nf}$ and $D_{ves,nf}$, obtained from colchicine treated cells, showing no persistent motion (green - F-actin, black – vesicles, also compare to Fig. 3). Dashed areas correspond to mean value ± sd. These values agree remarkably well with the extrapolated behavior for $v \rightarrow 0$ of the experimental data obtained from control cells (dashed lines). The horizontal dotted line corresponds to the estimated value of the thermal diffusion coefficient D_{TH} of the vesicles, characterizing their spontaneous fluctuation in the absence of any active process. D_{TH} is more than one order of magnitude smaller than typical values of D_{ves} measured in control cells.

Drechsler et al. Figure 3

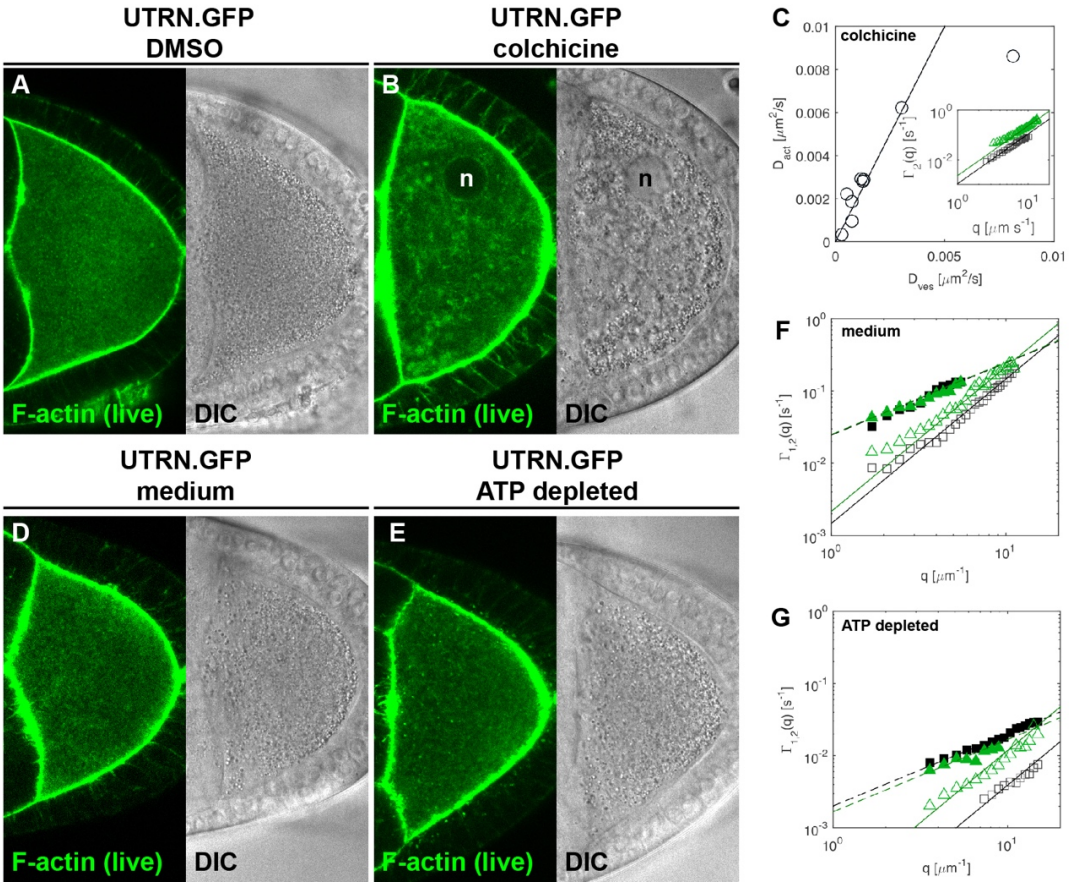

Figure 3. Microtubules and ATP are required for advection and active diffusion.

(A-C)* Persistent motion enhances active diffusion and depends on microtubules.** ***(A) UTRN.GFP (green, left panel) and DIC (right panel) images from living egg chambers, obtained from females fed with DMSO. ***(B)*** UTRN.GFP (green, left panel) and DIC (right panel) images from living egg chambers, obtained from females fed with colchicine. The efficiency of colchicine feeding was assured by using only cells that displayed a nucleus (n) detached from the anterior membrane (compared to nucleus positioning in Fig. 2A). Depolymerization of microtubules, and consequently the absence of flows, causes a heterogeneous distribution of vesicles (most obvious when comparing the DIC channels). At the same time, prominent actin filaments can be observed traversing the cytoplasm (see also Movie S2). ***(C)*** Diffusion coefficient of F-actin (D_{act}) as a function of the diffusion coefficient of vesicles (D_{ves}). In the absence of persistent flows the diffusivity of both, F-actin and vesicles, is reduced. However, the diffusion coefficients still maintain a linear relation with each other (solid line), with actin being always about a factor of two faster (continuous line corresponds to $D_{act} = 2D_{ves}$). This indicates a flow independent active diffusion process that affects vesicle movement and might be induced by actin itself. Each data point represents one cell. The inset shows the diffusive relaxation rates $\Gamma_2(q)$ measured for F-actin (green triangles) and vesicle (black boxes) in a

representative experiment on a single cell. Continuous lines are best fits to the data with a quadratic function.

(D-F)* Cytoplasmic motility is driven by active processes *(D) UTRN.GFP (green, left panel) and DIC (right panel) images from living egg chambers treated with control medium. ***(E)*** UTRN.GFP (green, left panel) and DIC (right panel) images from living egg chambers treated with sodium azide and 2-*D*-deoxyglucose to deplete ATP. Compared to controls, the distribution of vesicles and F-actin appears unchanged. However, the dynamics of all structures is greatly diminished (see also Movie S3). ***(F)*** $\Gamma_1(q)$ (empty symbols) and $\Gamma_2(q)$ (solid symbols) measured in a representative control cell (treated with medium). Green triangles correspond to F-actin, while gray squares correspond to vesicles. Continuous and dashed lines are best fits to the data with a quadratic or a linear function, respectively. ***(G)*** $\Gamma_1(q)$ and $\Gamma_2(q)$ obtained from ATP depleted cells plotted against the wave vector *q*. Color code as in panel (F). Compared to controls, the dynamics of ATP depleted cells is more than one order of magnitude slower.

Drechsler et al. Figure 4

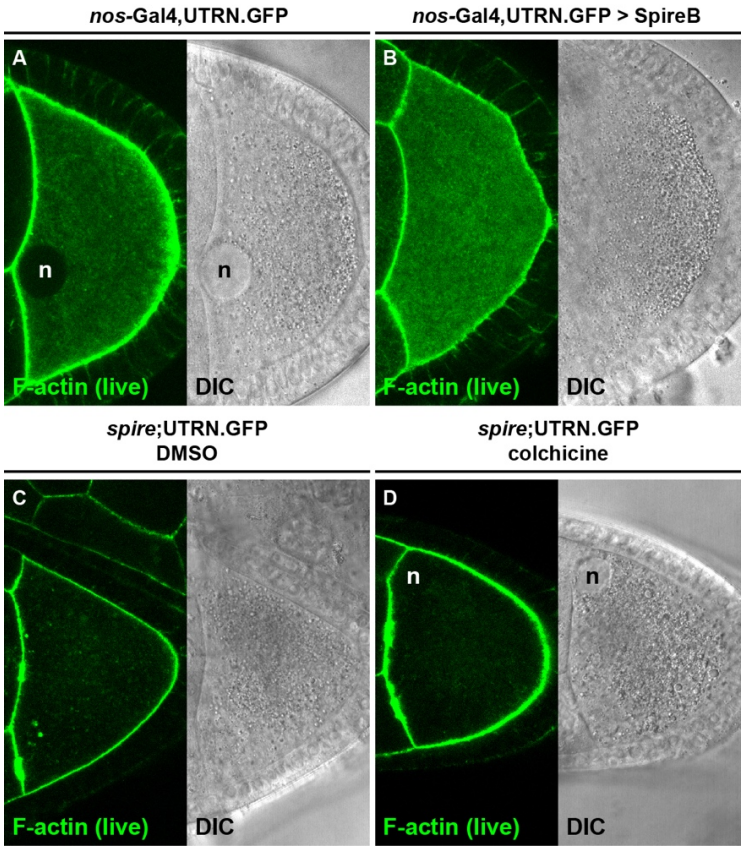

Figure 4. Cytoplasmic F-actin is the major source of active diffusion

(A) Living control egg chambers or ***(B)*** egg chambers over-expressing the actin nucleator SpireB. Overexpression of SpireB causes an increase in the amount of F-actin in the oocyte (see also Fig. S4). ***(C,D)*** *spire* mutant oocytes were incubated in control DMSO-containing medium ***(C)*** or in colchicine-containing medium ***(D)***. As expected, *spire* mutants do not form an actin mesh.